Journal of Southeast University (English Edition) Vol. 25, No. 3, pp. 351 – 355 Sept. 2009 ISSN 1003—7985

Enhanced hyperspectral imagery representation via diffusion geometric coordinates

He Jun Wang Qing Li Zigang

(School of Instrument Science and Engineering, Southeast University, Nanjing 210096, China)

Abstract: The concise and informative representation of hyperspectral imagery is achieved via the introduced diffusion geometric coordinates derived from nonlinear dimension reduction maps — diffusion maps. The huge-volume high-dimensional spectral measurements are organized by the affinity graph where each node in this graph only connects to its local neighbors and each edge in this graph represents local similarity information. By normalizing the affinity graph appropriately, the diffusion operator of the underlying hyperspectral imagery is well-defined, which means that the Markov random walk can be simulated on the hyperspectral imagery. Therefore, the diffusion geometric coordinates, derived from the eigenfunctions and the associated eigenvalues of the diffusion operator, can capture the intrinsic geometric information of the hyperspectral imagery well, which gives more enhanced representation results than traditional linear methods, such as principal component analysis based methods. For large-scale full scene hyperspectral imagery, by exploiting the backbone approach, the computation complexity and the memory requirements are acceptable. Experiments also show that selecting suitable symmetrization normalization techniques while forming the diffusion operator is important to hyperspectral imagery representation.

Key words: hyperspectral imagery; diffusion geometric coordinate; diffusion map; nonlinear dimension reduction

Hyperspectral sensors such as the airborne visible/infrared imaging spectrometer (AVIRIS), a NASA/Jet Propulsion Laboratory sensor, provide hyperspectral imagery in the form of hundreds of narrow and nearly continuous spectral bands. The spectrum recorded in each pixel of hyperspectral imagery is the measurement of solar radiation reflected by the Earth's surface. It has been investigated recently that there are many nonlinearities in hyperspectral imagery[1-3]; for example, in coastal environments, nonlinearities arise from the variable presence of water in pixels as a function of position in the landscape. And it has been pointed out that traditional linear data analysis tools, such as PCA and MNF[4], the de facto standards in the analysis of spectral data, cannot perform as we wish, because these methods make the assumption that the observed data are linearly correlated and they are blind to the nonlinearities lying in hyperspectral imagery.

In recent years, several well-known nonlinear modeling approaches based on manifold learning concepts have been developed. These approaches, such as ISOMAP[5], LLE[6], Laplacian eigenmaps[7], and diffusion maps[8], have a common assumption that data lie on or near a low dimensional manifold which is embedded in high dimensional Euclidean space. It is a great improvement on exploiting the intrinsic geometric information while modeling high dimensional datasets. Parameterization of a low dimensional manifold means obtaining concise coordinates representation. In the case of measuring the distance between two points of high dimensional space, by using this kind of coordinates, the distance is measured in the geometric way, which means that the distance is measured along the manifold rather than the straight line of Euclidean space.

As the nonlinear modeling mentioned above can efficiently exploit the nonlinear characteristics in the high dimensional data, recently some researchers[1-3] in the hyperspectral imagery analysis community have applied these approaches to coastal land-cover classification and hyperspectral segmentation applications. In Refs. [1-2], they chose ISOMAP as a powerful tool to exploit the manifold coordinates of hyperspectral imagery, as ISOMAP can guarantee global optimal coordinates compared with other methods. However, it is also proved that local approaches such as Laplacian eigenmaps and diffusion maps, under the conditions choosing exponential weights for the adjacency graph, lead to convergence of the graph Laplacian to the Laplace-Beltrami operator ΔM on the manifold[7,9-10]. These methods try to construct a weighted graph from the given data set, and via computing the eigenfunctions of the graph Laplacian, to induce the global coordinates of the underlying manifold.

Inspired by the successful work of Bachmann, we have also found that diffusion geometric coordinates computed by diffusion maps[8-9,11] can also be used for hyperspectral imagery representation, and realize almost the same quality as ISOMAP. Compared with the global manifold coordinates computed by ISOMAP, the potential advantage of diffusion geometric coordinates is more tractable computation complexity and memory requirements for large-size hyperspectral data, if we exploit the approximation nearest neighbor searching technique[12].

1 Diffusion Maps and Diffusion Geometric Coordinates

In Refs. [8-9, 11], the authors presented a diffusion process-based high dimensional data analysis framework. Diffusion geometric coordinates, derived from diffusion maps, can exploit the underlying geometries well, since in the diffusion space the data points are reorganized in such a way that the Euclidean distance corresponds to diffusion metrics. The basic idea of diffusion maps is explained as follows.

Received 2008-12-24.

Biographies: He Jun (1978—), male, graduate; Wang Qing (corresponding author), male, doctor, professor, wq_seu@seu.edu.cn.

Foundation item: The National Key Technologies R&D Program during the 11th Five-Year Plan Period (No. 2006BAB15B01).

Citation: He Jun, Wang Qing, Li Zigang. Enhanced hyperspectral imagery representation via diffusion geometric coordinates[J]. Journal of Southeast University (English Edition), 2009, 25(3): 351 – 355.

Let (Γ, A, μ) be a measure space, where Γ is a set whose points are abstract objects. The data points can be thought of as the nodes of a graph whose weight function $k(x, y)$ satisfies the following properties:

1) k is symmetric: $k(x, y) = k(y, x)$;

2) k is positivity preserving: for all x and y in Γ, $k(x, y) \geqslant 0$;

3) k is positive semi-definite: for all real-valued bounded functions f defined on Γ,

$$\iint_{\Gamma} k(x, y) f(x) f(y) \, \mathrm{d}\mu(x) \, \mathrm{d}\mu(y) \geqslant 0$$

where μ is a probability measure on Γ.

Usually, $k(x, y)$ is defined as a heat kernel, which means $k(x, y) = \mathrm{e}^{-(\|x-y\|^2/(2\varepsilon))}$. After normalizing the kernel appropriately referring to Refs. [9, 11], random walk can be defined on the underlying graph, and the naturally symmetric diffusion operator $\tilde{A}$ with the normalized kernel $\tilde{a}(x, y)$ can be defined as

$$\tilde{A}f(x) = \int_{\Gamma} \tilde{a}(x, y) f(y) \, \mathrm{d}\mu(y) \tag{1}$$

The following spectral decomposition can be induced on the diffusion operator $\tilde{A}$ by the spectral graph theory.

$$\tilde{a}(x, y) = \sum_{i \geqslant 0} \lambda_i^2 \phi_i(x) \phi_i(y) \qquad \lambda_0 = 1 \geqslant \lambda_1 \geqslant \lambda_2 \geqslant \cdots \tag{2}$$

where λ_i and $\phi_i(x)$ are the corresponding eigenvalue and eigenfunctions of the operator $\tilde{A}$. As for diffusion step m, also let $\tilde{a}^m(x, y)$ be the kernel of $\tilde{A}^m$, then the following equation also holds:

$$\tilde{a}(x, y) = \sum_{i \geqslant 0} \lambda_i^m \phi_i(x) \phi_i(y) \tag{3}$$

So the family of diffusion maps $\{\boldsymbol{\Phi}_m\}$ can be induced as

$$\boldsymbol{\Phi}_m(x) = \begin{Bmatrix} \lambda_0^m \phi_0(x) \\ \lambda_0^1 \phi_0(x) \\ \vdots \end{Bmatrix} \tag{4}$$

Coifman et al. [8] also pointed out that the link between diffusion maps and distances is

$$\| \boldsymbol{\Phi}_m(x) - \boldsymbol{\Phi}_m(y) \|^2 = \sum_{j \geqslant 0} \lambda_j^{2m} (\phi_j(x) - \phi_j(y))^2 = D_m^2(x, y) \tag{5}$$

which means that the diffusion map $\boldsymbol{\Phi}_m$ embeds the data into a Euclidean space in which the Euclidean distance is equal to the diffusion distance D_m. Moreover, the diffusion space can be accurately approximated by retaining only the terms when λ_j^{2m} remains numerically significant; therefore the embedding

$$x \xrightarrow{\text{embedding}} \tilde{\boldsymbol{x}} = \{\lambda_0^m \varphi_0(x), \lambda_1^m \varphi_1(x), \ldots, \lambda_{j_0}^m \varphi_{j_0}(x)\} \tag{6}$$

satisfies

$$D_m^2(x, y) = \|\tilde{\boldsymbol{x}} - \tilde{\boldsymbol{y}}\|^2 (1 + O(\mathrm{e}^{-\alpha m})) \tag{7}$$

Here, the embedding coordinates refer to diffusion geometric coordinates, since they capture the intrinsic geometries exploited by the diffusion process. In the next section we will use the diffusion geometric coordinates to represent hyperspectral imagery in a concise way while retaining more information than traditional linear methods.

2 Hyperspectral Imagery Representation via Diffusion Geometric Coordinates

A hyperspectral imagery I with width w, height h and n bands can be formally defined as a $w \times h$ matrix lying in $\mathbf{R}^n$. For the purpose of simplicity, here we ignore the spatial relationship between each point. However, since spatial coherence is the important information for hyperspectral imagery investigated in Ref. [3], this work will be done in the future.

We model hyperspectral imagery as a weighted graph $G(V, E)$. Here V is the set of vertices and each vertex denotes the original pixel of the hyperspectral imagery with n-band spectral reflectance. For example, given one hyperspectral imagery with 100×100 spatial resolution and 128 spectral bands, while forming the graph G, the size of vertices is 10^4 and each vertex corresponds to the original pixel with 128 spectral bands. In order to construct the weighted graph $G(V, E)$, we should also know the edge set E and then construct the affinity kernel according to the edge weights. Based on the motif "think locally, fit globally"[13] which is also the basic principle of diffusion maps, we only need to know the nearest neighbors of each vertex in its original spectral space. Given these vertices, finding the nearest neighbors by using the approximation nearest neighbor searching technique[12] is nearly of linear computation complexity. We connect each vertex to its nearest neighbors as edges and accordingly construct the affinity kernel.

Knowing the local neighbors of each vertex, we can fill in the weight matrix $\boldsymbol{W}$ between the vertex and its neighbors by computing the bump function of their similarities such as their spectral angle or traditional Euclidean distance since the local neighborhood we consider is assumed to be a linear subspace. For example, the weight w_{ij} between $\boldsymbol{p}_i$ and $\boldsymbol{p}_j$ can be computed by $w_{ij} = \mathrm{e}^{-(\|\boldsymbol{p}_i - \boldsymbol{p}_j\|^2/(2\varepsilon))}$, where $\|\boldsymbol{p}_i - \boldsymbol{p}_j\|$ denotes the local similarity measure. Since the diffusion geometric coordinates are the eigenvectors computed by the eigensolver from the weighted matrix, we must symmetrize this matrix in order to obtain the real eigenvectors. It is well known that one asymmetric matrix $\boldsymbol{W}$ can be symmetrized by adding its transpose $\boldsymbol{W}^{\mathrm{T}}$ or by dot multiplying its transpose $\boldsymbol{W}^{\mathrm{T}}$ and so on. Here we adopt the ADD symmetrization technique $\boldsymbol{W}_{\mathrm{sym}} = \boldsymbol{W} + \boldsymbol{W}^{\mathrm{T}}$. Experiments show that the symmetrization strategy affects final hyperspectral imagery representation significantly. We compare different strategies in the next section.

Next we normalize the symmetrized weighted matrix $\boldsymbol{W}_{\mathrm{sym}}$ to construct Markov random walk $\boldsymbol{W}_{\mathrm{rw}}$ on the underlying graph. Here we refer to $\boldsymbol{W}_{\mathrm{rw}}$ as the diffusion operator of the hyperspectral imagery. As discussed in the previous section, solving the eigenvectors $\{\varphi_0(x), \varphi_1(x), \ldots, \varphi_{j_0}(x)\}$ and the eigenvalues $(\lambda_0, \lambda_1, \ldots, \lambda_{j_0})$ of $\boldsymbol{W}_{\mathrm{rw}}$, we can obtain the family of diffusion maps $\{\boldsymbol{\Phi}_m\}$. Finally the diffusion geometric

coordinates of the hyperspectral imagery are obtained as

$$\{\lambda_0^m \varphi_0(x), \lambda_1^m \varphi_1(x), \ldots, \lambda_{j_0}^m \varphi_{j_0}(x)\} \tag{8}$$

So from the viewpoint of dimension reduction, we reduce the n-dimensional spectral space into j_0-dimensional diffusion space, and each pixel x_0 of the original hyperspectral imagery can be approximately represented by the diffusion geometric coordinate $\{\lambda_0^m \varphi_0(x_0), \lambda_1^m \varphi_1(x_0), \ldots, \lambda_{j_0}^m \varphi_{j_0}(x_0)\}$. Note that each diffusion component in expression (8) has just the same size entries corresponding to the size of the hyperspectral imagery with width w and height h, and we know that we have indexed each vertex according to its spatial location $\langle x, y \rangle$ as

$$e_{\text{idx}} = (y-1)w + x \tag{9}$$

Therefore, for each entry e_{idx} of the diffusion component $\lambda_i^m \phi_i$, we can restore the corresponding spatial location $\langle x, y \rangle$ of the image matrix by

$$\left.\begin{aligned} y &= \left\lceil \frac{e_{\text{idx}}}{w} \right\rceil \\ x &= e_{\text{idx}} - (y-1)w \end{aligned}\right\} \tag{10}$$

Compared with PCA-based methods, it can be seen from the former discussion that instead of computing correlations between all pixels we construct the graph from small local neighborhoods of each pixel. So the nonlinearities, in the form of hypersurfaces lying in the high dimensional spectral space, can be discovered by the simulated diffusion process on the underlying graph. Also note that given two arbitrary features $\boldsymbol{f}_1$ and $\boldsymbol{f}_2$ in the hyperspectral imagery, the diffusion distance $D_m(\boldsymbol{f}_1, \boldsymbol{f}_2)$ measures the intrinsic similarities between the two features. We can approximate $D_m(\boldsymbol{f}_1, \boldsymbol{f}_2)$ by computing $\|\hat{\boldsymbol{f}}_1 - \hat{\boldsymbol{f}}_2\|$ which means that we only keep the first few diffusion geometric coordinates $\hat{\boldsymbol{f}}_1 = \{\lambda_0^m \varphi_0(\boldsymbol{f}_1), \ldots, \lambda_{j_0}^m \varphi_{j_0}(\boldsymbol{f}_1)\}$ and $\hat{\boldsymbol{f}}_2 = \{\lambda_0^m \varphi_0(\boldsymbol{f}_2), \ldots, \lambda_{j_0}^m \varphi_{j_0}(\boldsymbol{f}_2)\}$. And the approximate error decays exponentially while the diffusion step m increases[11]. We use the following formula to evaluate the approximate error Δ,

$$\Delta = \frac{\left\| \|\hat{\boldsymbol{f}}_1 - \hat{\boldsymbol{f}}_2\| - D_m(\boldsymbol{f}_1, \boldsymbol{f}_2) \right\|}{D_m(\boldsymbol{f}_1, \boldsymbol{f}_2)} \tag{11}$$

Fig. 1 shows that when the diffusion step is large enough, only keeping the first few diffusion geometric coordinates, we can approximate $D_m(\boldsymbol{f}_1, \boldsymbol{f}_2)$ well.

As discussed in Refs. [1 − 2], usually each hyperspectral imagery is composed of more than 10^5 pixels, so one of the efficient ways to compute the whole imagery diffusion geometric coordinates is as follows: First, a feature representative backbone of the whole imagery is constructed and the backbone diffusion geometric coordinates are computed; secondly, the imagery is divided into several computing-tractable small tiles and the diffusion geometric coordinates of each tile are computed separately; finally, the alignment of the coordinates system of each tile to the common backbone diffusion geometric coordinates system is treated as one classic coordinate system transformation problem and the pseudoinverse method is used to solve it.

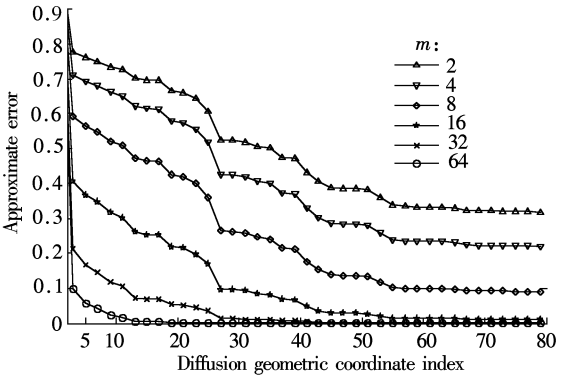

Fig. 1 Comparison of approximate error between different diffusion steps

Two remarks should also be stated here. One is that we will discard the first trivial eigenvalue and eigenvector because the nontrivial diffusion geometric coordinates, except the first component, give meaningful information of the underlying dataset. The other remark is that since we project the hyperspectral imagery on the first j_0 diffusion components, it is reasonable to view these j_0 components as new "bands"; that is to say, we will use these diffusion components to represent the hyperspectral imagery just as the original spectral bands do.

3 Experimental Results

The experimental hyperspectral imagery is Moffet Field Scene 2, obtained by AVIRIS in 1997[14]. There are 224 bands and about 30 bands containing unstructured noise in this imagery. So in our experiments, these bands are excluded, resulting in 194 bands. The resolution of the AVIRIS 194-band imagery is 614×512. Our experimental laptop is Intel Dual CPU 1.73 GHz, 2 GB memory and Windows Vista operation system.

We first select one 300×100 patch of the imagery to test our method. We set $K = 10$ to perform the nearest neighbor searching, and the ADD symmetrization technique $\boldsymbol{W}_{\text{sym}} = \boldsymbol{W} + \boldsymbol{W}^{\text{T}}$ is used to symmetrize the diffusion operator. The patch of the imagery is projected to the first 15 diffusion geometric coordinates. It takes 64.71 s to perform range search forming the kernel matrix with the size of $30\,000 \times 30\,000$, and takes 18.45 s to compute the eigenvectors and eigenvalues of the sparse diffusion operator. In Fig. 2, our method shows more superior representation results than traditional linear PCA-based methods which are calculated by OPTICKS[15]. Though the first principal components contain the most information after performing PCA transformation on hyperspectral imagery, almost every component consists of noise, and some components are contaminated too much to be recognized. So we carefully select the components with the highest SNR. Fig. 2(a) shows the original spectral image displayed wavelengths: 0.65 μm, 0.55 μm, 0.45 μm; Fig. 2(b) uses the linear PCA coordinates 1-9-7 for the same scene; Figs. 2(c) to (f) are represented by the diffusion geometric coordinates 2-3-4, 5-6-7, 8-9-10, and 11-12-13, respectively. Compared with linear PCA results, diffusion geometric coordinates show the extensive structure of the hyperspectral imagery, which are almost comparable to the global manifold coordinates derived from ENH-ISOMAP[1-2].

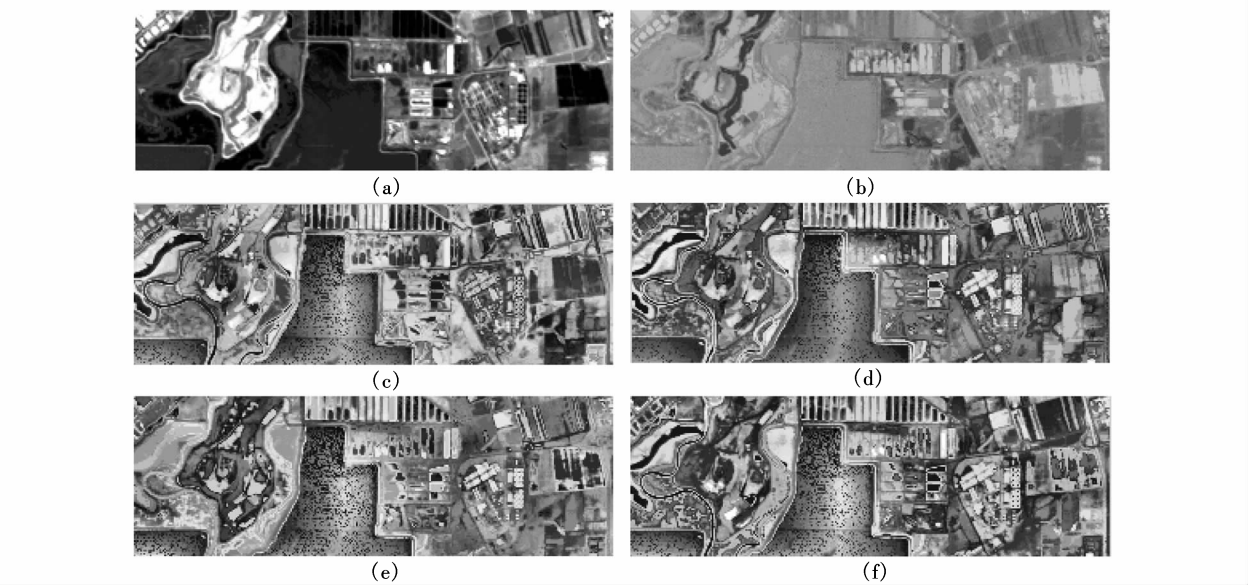

Fig. 2 Comparison of 300 × 100 patch of hyperspectral imagery representation between linear method and diffusion geometric coordinates approach. (a) RGB image 0.65, 0.55, 0.45 μm; (b) Linear PCA coordinates 1-9-7; (c) to (f) Diffusion geometric coordinates 2-3-4, 5-6-7, 8-9-10, and 11-12-13

Secondly, we experiment with different symmetrization techniques while forming the diffusion operator on the underlying hyperspectral imagery. It can be seen in Fig. 3 that the dot-multiplication symmetrization technique $\boldsymbol{W}_{\text{sym}} = \boldsymbol{W} \times \boldsymbol{W}^{\text{T}}$ (see Fig. 3(a)) and the multiplication symmetrization technique $\boldsymbol{W}_{\text{sym}} = \boldsymbol{W} \times \boldsymbol{W}^{\text{T}}$ (see Fig. 3(b)) exhibit more degenerated representation results than our adopting symmetrization method $\boldsymbol{W}_{\text{sym}} = \boldsymbol{W} + \boldsymbol{W}^{\text{T}}$. Here we demonstrate the RGB images of the diffusion geometric coordinates 2-3-4. The reason is that when we construct the affinity kernel, only knowing the nearest neighbors of each vertex will lead to the kernel matrix being really sparse, so forming the diffusion operator by matrix multiplication or dot multiplication will lead to the final diffusion operator being nearly singular. That is to say, the eigen-solved diffusion geometric coordinates on the diffusion operator by these symmetrization methods are not stable and contain significant numerical errors.

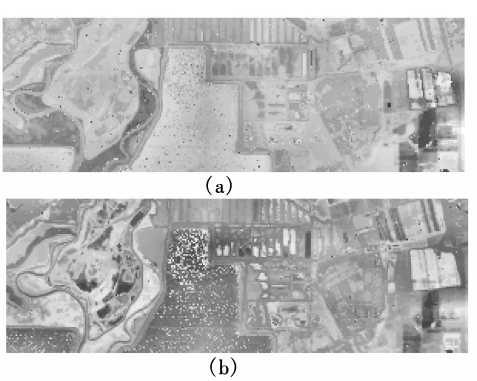

Fig. 3 Effects of different symmetrization methods on hyperspectral representation. (a) $\boldsymbol{W}_{\text{sym}} = \boldsymbol{W}. \times \boldsymbol{W}^{\text{T}}$; (b) $\boldsymbol{W}_{\text{sym}} = \boldsymbol{W} \times \boldsymbol{W}^{\text{T}}$

Finally, we extend the experiments to the whole 614 × 512 imagery via the so-called backbone approach[2]. In order to construct the feature-representative backbone of the whole scene, we randomly selected 15% points as the backbone, since in practice 10% to 33% random samples of the 10^5 to 10^6 size dataset can approximately represent the feature space well. It takes 95.6 s to compute the backbone diffusion geometric coordinates, and totally take 672 s to reconstruct the full scene coordinates. Fig. 4 shows the full scene RGB representation via diffusion geometric coordinates 5-6-7.

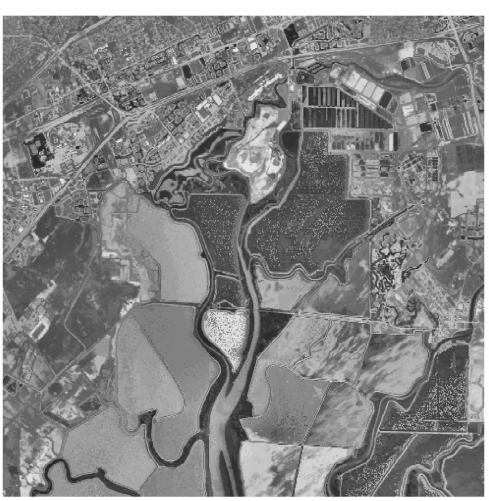

Fig. 4 Diffusion geometric coordinates 5-6-7 of the Moffet Field scene Ⅱ in 1997

4 Conclusion and Future Work

By the study of nonlinear dimension reduction, we find that the diffusion geometric coordinates can well represent hyperspectral imagery. Compared with linear methods, the approach presented in this paper has better feature separation ability and more scalable ability while dealing with larger imagery. We also investigate different symmetrization techniques while forming the diffusion operator on the hyperspectral imagery, which significantly affects the representation results.

Diffusion geometric coordinates exhibit great performance in modeling hyperspectral imagery, as they can suc-

cessfully capture the intrinsic geometries underlying high-dimensional data. However, some study still needs to be done. First, it has been shown in Ref. [16] that, while modeling complex structures such as graph and manifold, diffusion processes and Markov processes can be analyzed in a multiscale fashion. In this paper, we do not exploit the multiscale analysis ability of diffusion geometric coordinates. The relationship between multiscale diffusion and hyperspectral representation will be investigated in future work. Secondly, the spatial coherence should be considered while the diffusion operator is constructed. Finally, as for the backbone approach, since it is originated from semi-supervised learning methodology, more powerful and efficient semi-supervised manifold learning methods should be investigated further.

Acknowledgements He Jun is grateful for the fellowship support from the Institute for Pure and Applied Mathematics at the University of California, Los Angeles, which he was visiting while the experiments were conducted and part of this paper was written.

References

[1] Bachmann C M, Ainsworth T L, Fusina R A. Exploiting manifold geometry in hyperspectral imagery [J]. *IEEE Trans Geosci Remote Sens*, 2005, **43**(3): 441 - 454.

[2] Bachmann C M, Ainsworth T L, Fusina R A. Improved manifold coordinate representations of large-scale hyperspectral scenes [J]. *IEEE Trans Geosci Remote Sens*, 2006, **44**(10): 2786 - 2803.

[3] Mohan A, Sapiro G, Bosch E. Spatially coherent nonlinear dimensionality reduction and segmentation of hyperspectral images [J]. *IEEE Geosci Remote Sens Lett*, 2007, **4**(2): 206 - 210.

[4] Green A A, Berman M, Switzer P, et al. A transformation for ordering multispectral data in terms of image quality with implications for noise removal [J]. *IEEE Trans Geosci Remote Sens*, 1988, **26**(1): 65 - 74.

[5] Tenenbaum J B, Silva V, Langford J C. A global geometric framework for nonlinear dimensionality reduction [J]. *Science*, 2000, **290**(5500): 2319 - 2323.

[6] Roweis S T, Saul L K. Nonlinear dimensionality reduction by locally linear embedding [J]. *Science*, 2000, **290**(5500): 2323 - 2327.

[7] Belkin M, Niyogi P. Laplacian eigenmaps for dimensionality reduction and data representation [J]. *Neural Comput*, 2003, **15**(6): 1373 - 1396.

[8] Coifman R R, Lafon S, Lee A B, et al. Geometric diffusions as a tool for harmonic analysis and structure definition of data: diffusion maps [J]. *Proc of the National Academy of Sciences*, 2005, **102**(21): 7426 - 7431.

[9] Lafon S. Diffusion maps and geometric harmonics [D]. New Haven: Department of Mathematics of Yale University, 2004.

[10] Hein M, Audibert J Y, Luxburg U V. From graphs to manifolds-weak and strong pointwise consistency of graph Laplacians [C]//*Proc of the* 18*th Conference on Learning Theory* (*COLT*). Bertinoro, 2005: 470 - 485.

[11] Coifman R R, Lafon S. Diffusion maps [J]. *Appl Comput Harmon Anal*, 2006, **21**(1): 5 - 30.

[12] Arya S, Mount D M, Netanyahu N S, et al. An optimal algorithm for approximate nearest neighbor searching [J]. *J ACM*, 1998, **45**(6): 891 - 923.

[13] Saul L K, Roweis S T. Think globally, fit locally: unsupervised learning of low dimensional manifolds [J]. *J Mach Learn Res*, 2003, **4**(2): 119 - 155.

[14] AVIRIS [EB/OL]. (1997) [2008-05-30]. http://aviris.jpl.nasa.gov/html/aviris.instrument.html.

[15] Opticks [EB/OL]. (2007) [2008-06-30]. https://opticks.ballforge.net.

[16] Coifman R R, Maggioni M. Diffusion wavelets [J]. *Appl Comput Harmon Anal*, 2006, **21**(1): 53 - 94.

基于扩散几何坐标的高光谱影像的增强表示

何 军 王 庆 李滋刚

(东南大学仪器科学与工程学院,南京 210096)

摘要:利用扩散映射所诱导出的扩散几何坐标对高光谱影像低维可视化表示,这种非线性维度约简的表示方法能够得到高光谱影像紧凑而富含信息量的可视化表示结果。通过对海量高光谱影像中每个高光谱观测向量进行局部搜索,仅考虑局部的邻接性和局部的相似度,构造出该高光谱影像对应的近邻图;对近邻图进行合适的规范化,得到该高光谱影像对应的扩散算子,相当于利用该扩散算子对高光谱特征空间模拟出马尔可夫随机游走.因此这样的构造较好地把握了高光谱影像内蕴的几何信息,与传统的基于主成分分析的线性降维表示方法相比,由扩散算子的特征分解所诱导出的扩散几何坐标能够给出更好的表示效果,富含更多的信息.对于大尺度的全景高光谱影像,利用构造"骨干"扩散几何坐标系的方法,其计算的时间复杂性和空间需求都是可接受的.实验也表明,选择合适的对称化方法规范扩散算子对于最终的高光谱影像表示有重要的影响.

关键词:高光谱影像;扩散几何坐标;扩散映射;非线性维度约简

中图分类号:TP391